Both major xanthophyll cycles present in nature can provide Non-Photochemical Quenching in the model diatom *Phaeodactylum tricornutum*

Chiara E. Giossi[a]*, Marie A. Wünsch[a,c], Oliver Dautermann[b], Alexander F. Schober[a,d], Jochen M. Buck[a], Peter G. Kroth[a], Martin Lohr[b]*, Bernard Lepetit[a,c]*

[a] Department of Biology, University of Konstanz, 78464 Konstanz, Germany

[b] Institute of Molecular Physiology, Johannes Gutenberg University, 55099 Mainz, Germany

[c] Present address: Institute of Life Sciences, University of Rostock, 18059 Rostock, Germany

[d] Present address: School of Biological Science, Nanyang Technological University, 637551 Singapore

***To whom correspondence may be addressed:**

chiara.giossi@uni-konstanz.de, lohr@uni-mainz.de, bernard.lepetit@uni-rostock.de

Keywords: diatoms, non-photochemical quenching (NPQ), photoprotection, xanthophyll cycle

Abstract

Xanthophyll cycling contributes to photoprotection by regulating Non-Photochemical Quenching (NPQ). While most photosynthetic eukaryotes including land plants use the violaxanthin cycle, some algae like diatoms and haptophytes rely on the diadinoxanthin cycle for photoprotection. These algae also contain minor amounts of violaxanthin cycle pigments, serving as precursors in xanthophylls biosynthesis. Both cycles are catalyzed by the enzymes violaxanthin de-epoxidase (VDE) and zeaxanthin epoxidase (ZEP). Here, we characterized the role of *VDE* and different ZEP-encoding paralogs (*ZEP2* and *ZEP3*) in the model diatom *Phaeodactylum tricornutum*. While knockout of *VDE* and *ZEP3* significantly impaired the diadinoxanthin cycle, lack of *ZEP2* led to

sustained accumulation of the violaxanthin cycle instead of diadinoxanthin cycle pigments under high irradiance, with no negative effect on NPQ capacity. We demonstrate that both major xanthophyll cycles present in nature can function with comparable efficiency within the same species, offering a new perspective on the evolution of xanthophyll-mediated photoprotection.

Introduction

Diatoms are amongst the main primary producers on Earth (Field et al., 1998; Falkowski et al., 2004), dominating phytoplankton and microphytobenthic communities in nutrient-rich turbulent waters where irradiance can change very rapidly due to daily fluctuations and to the movement of water and sediments (Tozzi et al., 2004; Lavaud, 2007). To cope with this highly dynamic light stress and avoid the formation of reactive oxygen species and consequent photoinhibition, diatoms have evolved different photoprotection strategies (Lavaud et al., 2007; Kan et al., 2023). One of these is Non-Photochemical Quenching (NPQ), a ubiquitous multi-component mechanism that dissipates the surplus of excitation energy as heat, thus preventing the over-saturation of the photosynthetic apparatus (Takahashi and Badger, 2011; Domingues et al., 2012; Goss and Lepetit, 2015; Bassi and Dall'Osto, 2021). qE, or high energy-state quenching, is fastest component of NPQ, taking place in the light-harvesting complexes of photosystem II (PSII) (Takahashi and Badger, 2011; Domingues et al., 2012; Goss and Lepetit, 2015; Bassi and Dall'Osto, 2021). In diatoms, this mechanism relies on antenna proteins of the Lhcx family (Bailleul et al., 2010; Lepetit et al., 2017; Buck et al., 2019; Buck et al., 2021).

In most photosynthetic eukaryotes, the on- and offset of qE is regulated by the xanthophyll cycle, a rapid interconversion of carotenoids that relies on removal or addition of epoxy groups (Latowski et al., 2011). Two major xanthophyll cycles exist in nature (Latowski et al., 2011; Goss and Lepetit, 2015): i) the violaxanthin (Vx) cycle, a two-step reaction involving Vx, antheraxanthin (Ax) and zeaxanthin (Zx), present in green algae, land plants and several classes of heterokont algae; and ii) the diadinoxanthin (Dd) cycle, responsible for the interconversion of only

58 two pigments, Dd and diatoxanthin (Dt), found in haptophytes and other
59 heterokonts (including diatoms). Both cycles are tightly regulated via light-
60 dependent changes in the trans-thylakoidal ΔpH (Latowski et al., 2011; Goss and
61 Lepetit, 2015). In diatoms, the light induced ∆pH activates the enzyme violaxanthin
62 de-epoxidase (VDE), converting Dd into Dt and thus triggering qE. When light
63 stress and ∆pH are relaxed, Dt is converted back to Dd by the enzyme zeaxanthin
64 epoxidase (ZEP), completing the cycle and thus abolishing qE (Goss et al., 2006a;
65 Blommaert et al., 2021). Similarly, in plants and algae displaying the Vx cycle qE
66 is triggered by the de-epoxidation of Vx to Zx through the intermediate Ax, and Vx
67 is restored by the re-epoxidation of Zx (Latowski et al., 2011). Interestingly,
68 diatoms and other algae using the Dd cycle can accumulate pigments of the Vx
69 cycle under extreme irradiance (Lohr and Wilhelm, 1999; Lohr and Wilhelm, 2001;
70 Kuczynska et al., 2020). This was explained by the essential role of Vx as
71 intermediate in the biosynthesis of Dd and fucoxanthin (Lohr, 2011; Dambek et al.,
72 2012). However, it is unclear whether Zx and Ax can also trigger NPQ in diatoms.
73 Diatoms possess multiple paralogs encoding for potential xanthophyll cycle
74 enzymes, originated via gene duplication (Coesel et al., 2008; Frommolt et al.,
75 2008). In the model diatom *Phaeodactylum tricornutum*, the role of ZEP1, VDL1
76 and VDL2 in the fucoxanthin biosynthetic pathway has been recently elucidated
77 (Dautermann et al., 2020; Bai et al., 2022). Hence, the photoprotective function
78 must be provided by other paralogs such as *VDE*, *VDR, ZEP2* and/or *ZEP3*.
79 Indeed, RNA silencing (Lavaud et al., 2012) and recombinant protein experiments
80 (Bojko et al., 2013; Olchawa-Pajor et al., 2019) pointed to VDE as the major
81 regulator of Dd de-epoxidation in *P. tricornutum*. Moreover, *VDE* and *ZEP3* are
82 arranged in a gene cluster conserved in *P. tricornutum* and other diatom lineages,
83 suggesting shared evolutionary history and conserved functions (Frommolt et al.,
84 2008; Bai et al., 2022). Thus, VDE and ZEP3 could be the main regulators of the
85 Dd cycle in *P. tricornutum*. On the contrary, ZEP2 may have an essential role in
86 other photoprotection mechanisms and/or carotenoid biosynthesis (Wilhelm et al.,
87 2006; Frommolt et al., 2008; Kuczynska et al., 2020).
88 In this work, we investigated the role of three xanthophyll cycle enzymes (ZEP2,

ZEP3 and VDE) in the Dd and Vx cycle in *P. tricornutum* through the respective knockout mutants. Our results highlight VDE and ZEP3 as major drivers of the Dd cycle: the VDE-deficient mutant (*vde KO*) was completely Dd cycle-deficient, while the ZEP3-deficient mutant (*zep3 KO*) did not rapidly re-epoxidize Dt after light stress. ZEP2-deficient mutants (*zep2 KO*) accumulated significantly large amounts of Zx and Ax under high light, at the expense of Dt; nevertheless, their NPQ capacity was comparable to the *wild type* (wt). This proves for the first time that both major xanthophyll cycles present in nature can provide NPQ in the same organism and suggests that Dt and Zx/Ax can contribute to the on- and offset of qE with comparable efficiency in diatoms.

Results

Knockouts of VDE and ZEP3 impair photoprotective xanthophyll cycling, while lack of ZEP2 enhances the accumulation of Vx cycle pigments in response to high light (HL). We generated knockout mutants for *ZEP2*, *ZEP3* and *VDE* throug CRISPR-Cas 9 approach (**Supplemental Note S1**). When grown under continuous low light (LL), no major differences in pigment content were observed between all newly generated mutant lines and wt (**Supplemental Table S2**).

However, after 5 days of 6 h HL:18 h LL regime each mutant displayed differences in xanthophyll cycling when compared to wt (**Fig. 1, Supplemental Fig. S5-S7**). In the wt, Dd slightly decreased after 6h of HL, concomitant with a massive Dt increase. In addition, minor amounts of Zx accumulated. During the following 30 min of recovery in LL, Dt and Zx were almost entirely epoxidized back to Dd and Vx. As expected, *vde KO* did not accumulate Dt or Zx during 6h of HL, but instead showed a strong increase of Dd and a small but statistically significant increase in Vx. Conversely, *zep3 KO* accumulated the highest amount of Dt under HL but was not able to convert it back to Dd during LL recovery. Finally, *zep2 KO* displayed the Dd cycle in response to changing light, but these pigments were present in significantly lower amounts compared to wt. Instead, this mutant was accumulating and cycling Vx cycle pigments to a much higher extent than all other strains: Zx

accumulated in response to 6h of HL and then decreased during the early stages of recovery (5 min of LL), while a transient pool of Ax accumulated; after 30min of LL, Vx accumulated at the expense of both Zx and Ax.

The phenotypes described for all mutants were reverted to wt in mutant lines complemented with the respective native genes under native promoters (**Supplemental Fig. S8-10**).

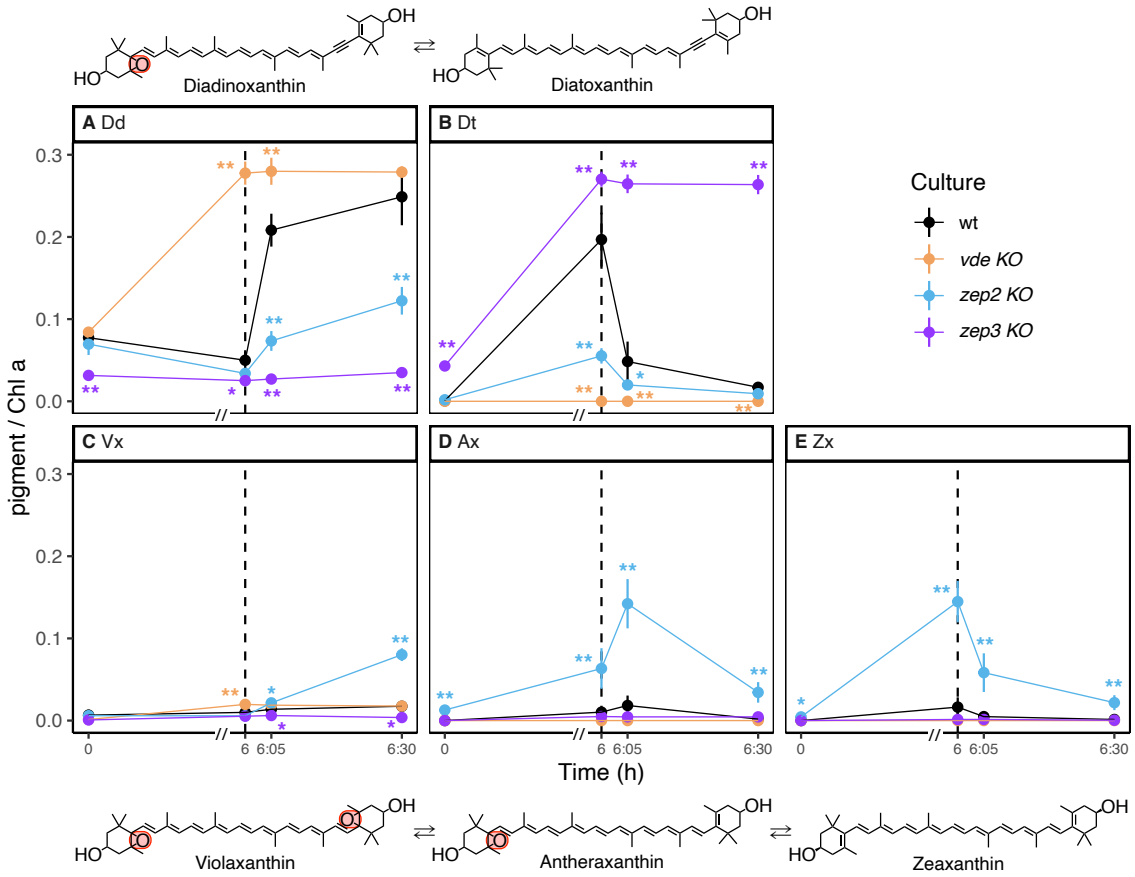

Fig. 1. Content of Dd and Vx cycle pigments in wt, *vde KO*, *zep2 KO* and *zep3 KO* after 5 days of HL:LL regime (average ± sd, n=3). Pigment content is expressed as pigment:chlorophyll *a* ratio (mol/mol). Time 0 is defined as the beginning of the HL phase (i.e. the sampling point in LL that immediately precedes the onset of HL on the fifth day of HL:LL treatment). The 6 h of HL phase and 30 min of recovery phase (LL) are separated with a dashed line. On the x-axis, recovery phase (from 6 to 6:30 h) was artificially enlarged to allow better visualization; axis break is indicated by a double dash (//). (*A*) diadinoxanthin; (*B*) diatoxanthin; (*C*) violaxanthin; (*D*) antheraxanthin; (*E*) zeaxanthin. Epoxy groups are highlighted with a red rectangle. Statistical significance marks indicate significant differences between the corresponding mutant line and wt at each time point,

135 according to adjusted p-value of multiple comparison t-test (*: $p < 0.05$; **: $p < 0.005$).

136 ***De novo* synthesis drives the light-induced accumulation of photoprotective**
137 **xanthophylls in all mutants, with no effect on the total pigment pool.** After 6 h
138 of HL, *vde KO* and *zep3 KO* displayed no major difference in total Dd+Dt pool
139 compared to wt (**Fig. 2A**), and in all three lines the Vx cycle pool was almost absent
140 (**Fig. 2B**). In contrast, *zep2 KO* displayed a much lower Dd+Dt content (about 20%
141 of the total xanthophyll cycle pigments, **Fig. 2A**) and instead accumulated a
142 massive total pool of Vx+Ax+Zx (about 80% of the total, **Fig. 2B**). All investigated
143 lines approximatively tripled their total xanthophyll cycle pigment content, with no
144 significant difference between each mutant and wt (**Fig. 2C**). This suggests that
145 the rate of de-novo biosynthesis of carotenoids is not affected by any of the target
146 mutations, thus being likely regulated in the same way in all investigated lines.
147 Previous studies suggested that *de novo* synthesis from β-carotene (rather than
148 the catabolism of other major carotenoids) is responsible for the high light-induced
149 accumulation of Zx in *P. tricornutum* (Lohr and Wilhelm, 1999) as in other algae
150 (e.g., *Chlamydomonas reinhardtii* (Baroli et al., 2003)). Accordingly, we observed
151 no significant differences in fucoxanthin content under different light conditions
152 between all investigated mutants and wt (**Fig. S7**), thus confirming that *de novo*
153 synthesis supplements xanthophyll cycle pigments during high light.
154 To further investigate the function-related accumulation of specific xanthophylls,
155 we calculated the total pool of epoxidized (**Fig. 2D**) and de-epoxidized pigments
156 (**Fig. 2E**). In response to 6 h of HL, *vde KO* accumulated a significantly higher
157 amount of epoxidized xanthophylls, while these were almost absent in *zep3 KO*.
158 Instead, *zep3 KO* accumulated a significantly higher amount of de-epoxidized
159 pigments. Despite the strong differences in the individual amounts of Vx and Dd
160 cycle pigments (**Fig. 1**), *zep2 KO* did not display significant differences in the total
161 pools of epoxidized or de-epoxidized xanthophylls throughout the light treatments
162 compared to wt (**Fig. 2E**).

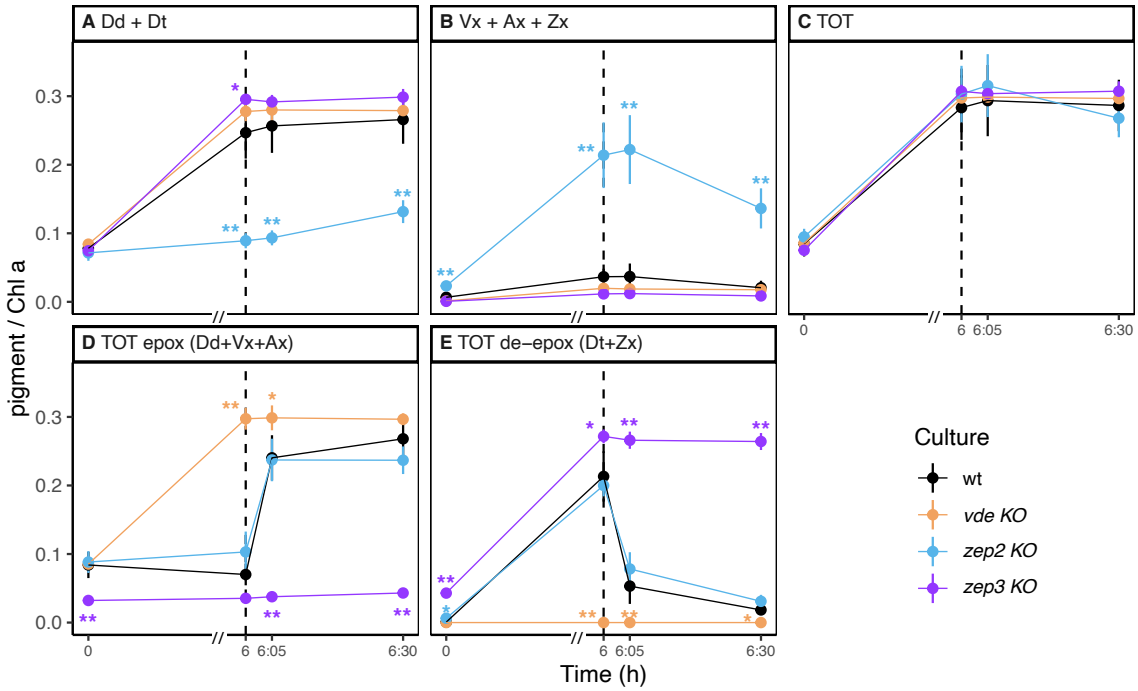

Fig. 2. Total pools of Dd and Vx cycle pigments in wt, *vde KO*, *zep2 KO* and *zep3 KO* after 5 days of HL:LL regime (average ± sd, n=3). Pigment content is expressed as pigment:chlorophyll *a* ratio (mol/mol). Time 0 is defined as the beginning of the HL phase (i.e. the sampling point in LL that immediately precedes the onset of HL on the fifth day of HL:LL treatment). The 6 h of HL phase and 30 min of recovery phase (LL) are separated with a dashed line. On the x-axis, recovery phase (from 6 to 6:30 h) was artificially enlarged to allow better visualization; axis break is indicated by a double dash (//). (*A*) total pool of Dd cycle pigments (diadinoxanthin + diatoxanthin); (*B*) total pool of Vx cycle pigments (violaxanthin + antheraxanthin + zeaxanthin); (*C*) sum of all Dd and Vx cycle pigments; (*D*) total pool of epoxidized pigments across different xanthophyll cycles (diadinoxanthin + violaxanthin + antheraxanthin); (*E*) total pool of de-epoxidized pigments across different xanthophyll cycles (diatoxanthin + zeaxanthin). Statistical significance marks indicate significant differences between the corresponding mutant line and wt at each time point, according to adjusted p-value of multiple comparison t-test (*: $p < 0.05$; **: $p < 0.005$).

Diversification of ZEP2 and ZEP3 uncouples *de novo* xanthophyll biosynthesis from xanthophyll cycling. Previously, ZEP2 had been indicated as main candidate for driving Dt epoxidation, based on the strong accumulation of monoepoxides (Ax and lutein epoxide) in a ZEP-deficient *npq2* mutant of *Arabidopsis thaliana* stably transformed with *ZEP2* from *P. tricornutum* (Eilers et al., 2016). Our results however demonstrate that ZEP3 is the ZEP isoform mainly

183 co-regulating the Dd cycle with VDE in *P. tricornutum*. This is consistent with the
184 clustered organization of *VDE* and *ZEP3* within the genomes of *P. tricornutum* and
185 various other diatoms (Coesel et al., 2008; Frommolt et al., 2008; Bai et al., 2022),
186 with several reports of their correlated expression pattern under light stress
187 (Coesel et al., 2008; Nymark et al., 2009; Kuczynska et al., 2020; Kan et al., 2023).
188 The function of ZEP3 was also recently confirmed in other independent studies
189 (Ware et al., 2024; Græsholt et al., 2024).
190 Although *zep3 KO* accumulated high amounts of Dt during HL, the mutant was
191 almost devoid of Dt before the onset of HL on the 5th day of light stress regime
192 (**Fig. 1**, Time = 0 h), indicating that Dt epoxidation could still be performed in this
193 mutant on longer time scales. Transient expression of *ZEP2* or *ZEP3* from *P.*
194 *tricornutum* in the ZEP-deficient *aba2* mutant of *Nicotiana plumbaginifolia* lacking
195 epoxy xanthophylls resulted in almost identical pigment phenotypes accumulating
196 Vx, neoxanthin and lutein epoxide (**Supplemental Fig. S11**), indicating that both
197 isoforms can accept the same xanthophylls as substrate and therefore allow
198 epoxidation of Zx as well as Dt. ZEP2 is thus likely responsible for the long-term
199 re-epoxidation of Dt and Zx in *zep3 KO* following HL exposure, although hardly
200 any epoxidation activity was detectable during the first 30 min of recovery. A major
201 contribution of carotenoid degradation to the scavenging of Dt in the *zep3 KO*
202 during prolonged LL recovery appears unlikely, since carotenoid catabolism is
203 dampened under lower irradiances (Biswal, 1995; Steiger et al., 1999).
204 These observations suggest that ZEP2 and ZEP3 have overlapping but not
205 completely redundant functions. As we reported similarly broad substrate
206 specificities in tobacco (**Supplemental Fig. S11**), we conclude that this difference
207 is most likely not based on substrate preferences of the two enzymes. We propose
208 that *P. tricornutum* separates photoprotective xanthophyll cycling from *de novo*
209 biosynthesis between ZEP3 and ZEP2 respectively, either through functional
210 specialization and/or physical separation of the two isoforms (**Fig. 3**). A detailed
211 version of these models, illustrating the relationship between predicted enzyme
212 function and observed phenotypes is presented in **Fig. S12**.

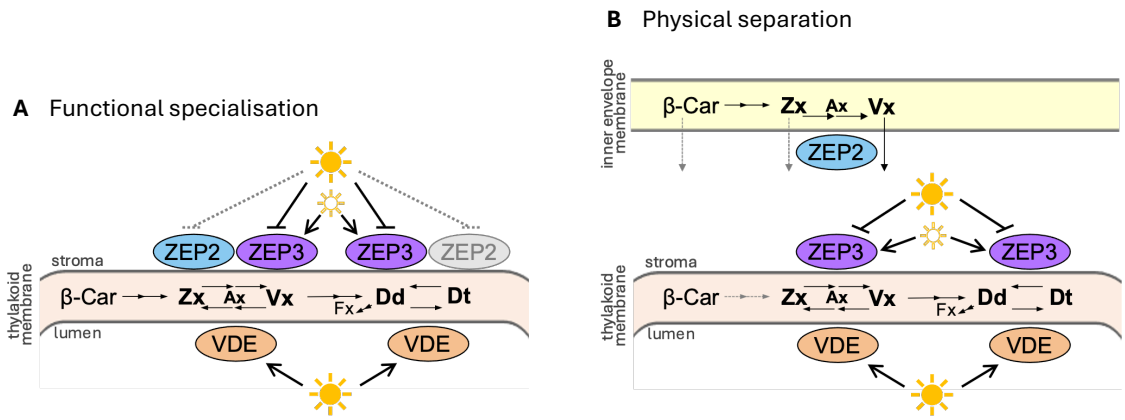

Fig. 3. Two models explaining the separation of *de novo* xanthophyll biosynthesis from photoprotective xanthophyll cycling in *P. tricornutum*. In both models, ZEP2 is mostly responsible for *de novo* biosynthesis, while ZEP3 mostly controls photoprotective xanthophyll cycling as antagonist of VDE. (*A*) Functional specialization of ZEP2 and ZEP3. Activity of ZEP3 is maximal under lower irradiances (represented by a hollow sun) and minimal at higher irradiances (represented by a sun), while VDE activity is maximum at higher irradiances. In contrast, ZEP2 is constitutively active, although less efficient than ZEP3 at least for Dt epoxidation. (*B*) In the physical separation model, the two processes are localized in different areas of the chloroplast stroma. Namely, *de novo* biosynthesis of Vx from Zx is catalyzed by ZEP2, confined mostly at the inner envelope, while photoprotective xanthophyll cycling is regulated by ZEP3, located mostly at the thylakoid membrane.

Despite a decreased Dd+Dt pool, *zep2 KO* displays wt-like NPQ capacity. To investigate the physiological effects of Vx cycle pigments accumulation in *zep2 KO*, the experiment was repeated with an increased number of time points during recovery phase, and pigment analysis was coupled with NPQ measurements. To exclude the influence of the so-called “dark NPQ” (i.e., the formation of NPQ in the dark, typical of diatoms (Goss et al., 2006a; Grouneva et al., 2009)) we used the maximum fluorescence measured in LL (0 h) as Fm for NPQ calculation, which is the common approach in diatoms in contrast to plants as low irradiance represents the condition at which maximum relaxation is achieved (Lepetit et al., 2013).

HPLC analysis confirmed the *zep2 KO* phenotype observed in the first set of experiments (**Fig.1-2**), both in terms of xanthophyll cycle pigments (**Fig. 4A-E**) and total pools (**Supplemental Fig. S9**). The additional time points improved the

resolution of the Vx cycle kinetics (**Fig. 4C-E**): while Zx decreased immediately after the cultures were switched from HL to LL, Ax transiently increased and peaked around 10 min of recovery, and then decreased in favor of an increase of Vx.

Analysis of epoxidation kinetics during LL recovery (**Fig. 5**) showed that Zx and Dt were epoxidized with similar rates within each algal strain, despite *zep2 KO* displayed lower rates for both reactions compared to the wt.

Despite a strongly reduced accumulation of Dd cycle pigments during HL (**Fig. 4A-B**), *zep2 KO* still generated the same NPQ as wt (**Fig. 4F**). While NPQ relaxation was initially slower in the mutant, as evidenced by the analysis of qE relaxation kinetics (**Fig. 5A**), no significant differences were observed after 30 min of recovery, indicating that *zep2 KO* was able to relax its NPQ with an efficiency comparable to the wt. These results were confirmed with a second independent *ZEP2* deficient mutant and a wt-like phenotype was restored for *zep2 KO* after complementation with native *ZEP2* (**Supplemental Fig. S9-10**). The same analysis performed on *zep3 KO* showed that the lack of Dt epoxidation during recovery directly corresponds to a lack of NPQ relaxation and a persisting quenching state (**Supplemental Fig. S13-S14**), thus confirming the role of this enzyme as main isoform for the recovery of the Dd cycle.

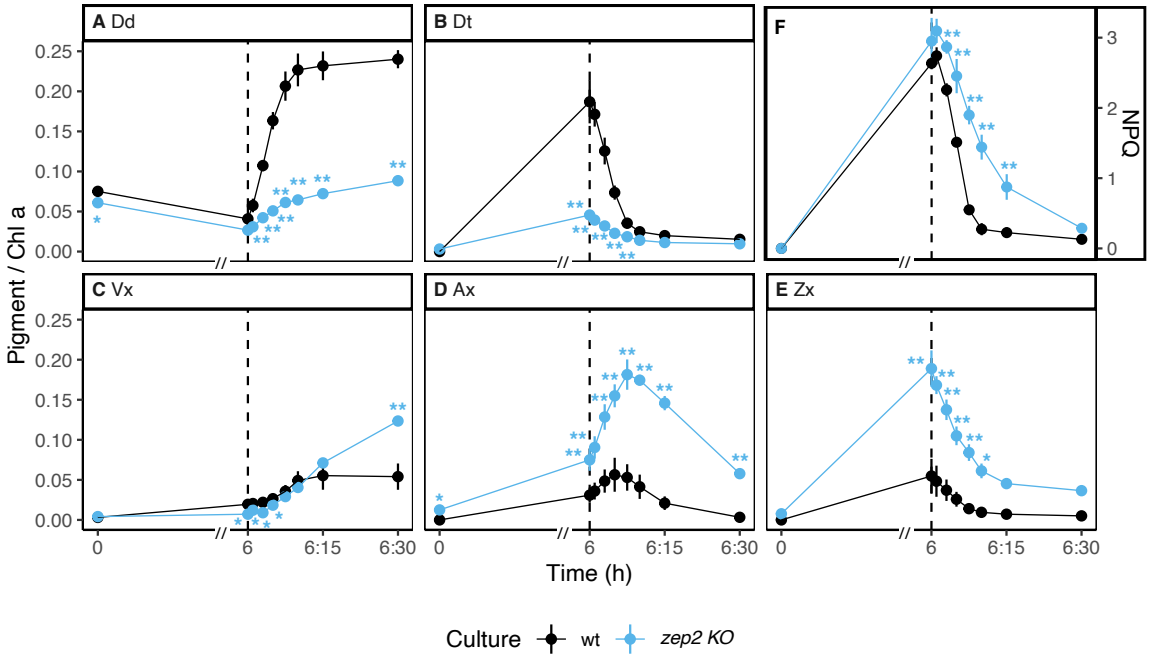

256

257 **Fig. 4. Pigment content of Dd and Vx cycle pigments coupled with NPQ analysis in wt and**
258 ***zep2 KO* after 5 days of HL:LL regime (average ± sd, n=3).** Pigment content is expressed as
259 pigment:chlorophyll *a* ratio (mol/mol). Time 0 is defined as the beginning of the HL phase (i.e. the
260 sampling point in LL that immediately precedes the onset of HL on the fifth day of HL:LL treatment).
261 The 6 h of HL phase and 30 min of recovery phase (LL) are separated with a dashed line. On the
262 x-axis, recovery phase (from 6 to 6:30 h) was artificially enlarged to allow better visualization; axis
263 break is indicated by a double dash (//). (*A*) diadinoxanthin; (*B*) diatoxanthin; (*C*) violaxanthin; (*D*)
264 antheraxanthin; (*E*) zeaxanthin; (*F*) NPQ. Statistical significance marks indicate significant
265 differences between the corresponding mutant line and wt at each time point, according to adjusted
266 p-value of multiple comparison t-test (*: $p < 0.05$; **: $p < 0.005$).

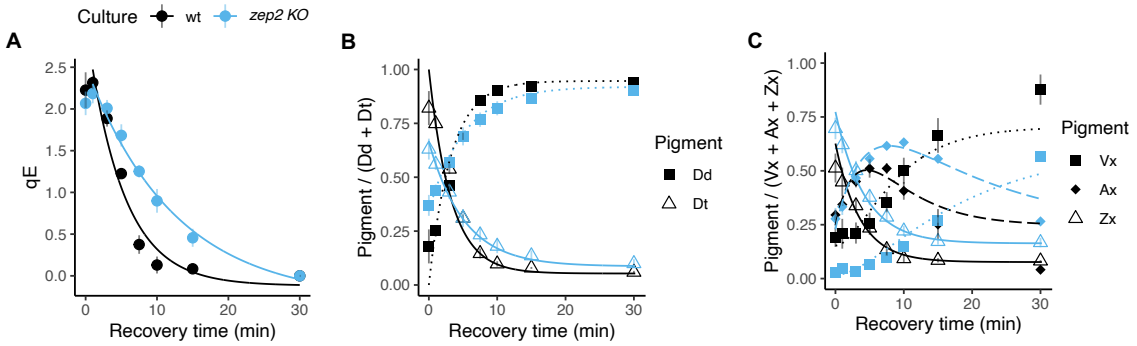

D

	qE	Dt → Dd	Zx → Ax	Ax → Vx	Ratios					
	R0	k_T [min^{-1}]	k_Z [min^{-1}]	k_A [min^{-1}]	k_T/k_Z	k_Z/k_T	k_T/k_A	k_A/k_T	k_Z/k_A	k_A/k_Z
wt	- 0.197 ± 0.025	0.310 ± 0.017	0.280 ± 0.035	0.167 ± 0.076	1.11 ± 0.08	0.90 ± 0.06	2.10 ± 0.81	0.53 ± 0.22	1.87 ± 0.61	0.58 ± 0.22
zep2 KO	- 0.081 ± 0.010	0.193 ± 0.012	0.237 ± 0.015	0.058 ± 0.003	0.82 ± 0.02	1.22 ± 0.03	3.31 ± 0.03	0.30 ± 0.003	4.06 ± 0.10	0.25 ± 0.01

Fig. 5. First order kinetics of qE recovery and of re-epoxidation of xanthophyll cycle pigments in wt and *zep2 KO* during 30 min of recovery phase after HL (average ± sd, n=3). (*A*) recovery rates of qE; (*B*) epoxidation of diadinoxanthin (Dd) to diatoxanthin (Dt); (*C*) epoxidation of zeaxanthin (Zx) via antheraxanthin (Ax) to violaxanthin (Vx); (*D*) corresponding rate constants of: qE recovery (R0); Dt to Dd epoxidation (k_T);, Zx to Ax epoxidation (k_Z); Ax to Vx epoxidation (k_A).

The Vx cycle can function as NPQ catalyst in *P. tricornutum*. In most diatoms, qE displays a robust linear correlation to the amount of Dt when no significant amounts of Vx cycle pigments are present (Goss et al., 2006a; Blommaert et al., 2021; Croteau et al., 2021). To factor in the presence of both distinct pools of de-epoxidized xanthophylls, we performed five different calculations of the de-epoxidized pigment pools possibly contributing to NPQ and analyzed their correlation with measured qE (**Fig. 6**).

Dt showed a clear linear relationship with qE in the wt (**Fig. 6A**), while this was much weaker in *zep2 KO*. The opposite was observed with Zx (**Fig. 6B**). In both cases, wt and *zep2 KO* displayed a completely different correlation pattern, noticeable by the poor fit of the combined linear model (i.e., including data points from both wt and *zep2 KO*). With the sum of Dt and Zx (**Fig. 6C**), model fit improved and the slopes of the linear regression for wt and mutant began to converge. The linear fit strongly improved when summing Dt, Zx and ½ Ax (**Fig. 6D**): models for

both *zep2 KO* and wt converged towards the general linear model, with the highest R^2 values. This indicates that the size of this specific pigment pool correlates with qE in a similar manner between these strains. Moreover, the addition of the full Ax pool (**Fig. 6E**) yielded a poorer fit for all investigated lines (with a notable decrease in R^2 values). We conclude that the sum of Dt, Zx and ½ Ax most adequately describes the xanthophyll cycle-dependent component of NPQ in HL-acclimated *P. tricornutum*. We further confirmed these results with a second *ZEP2* deficient mutant and complementation of *zep2 KO* with native *ZEP2* (**Supplemental Fig. S15**).

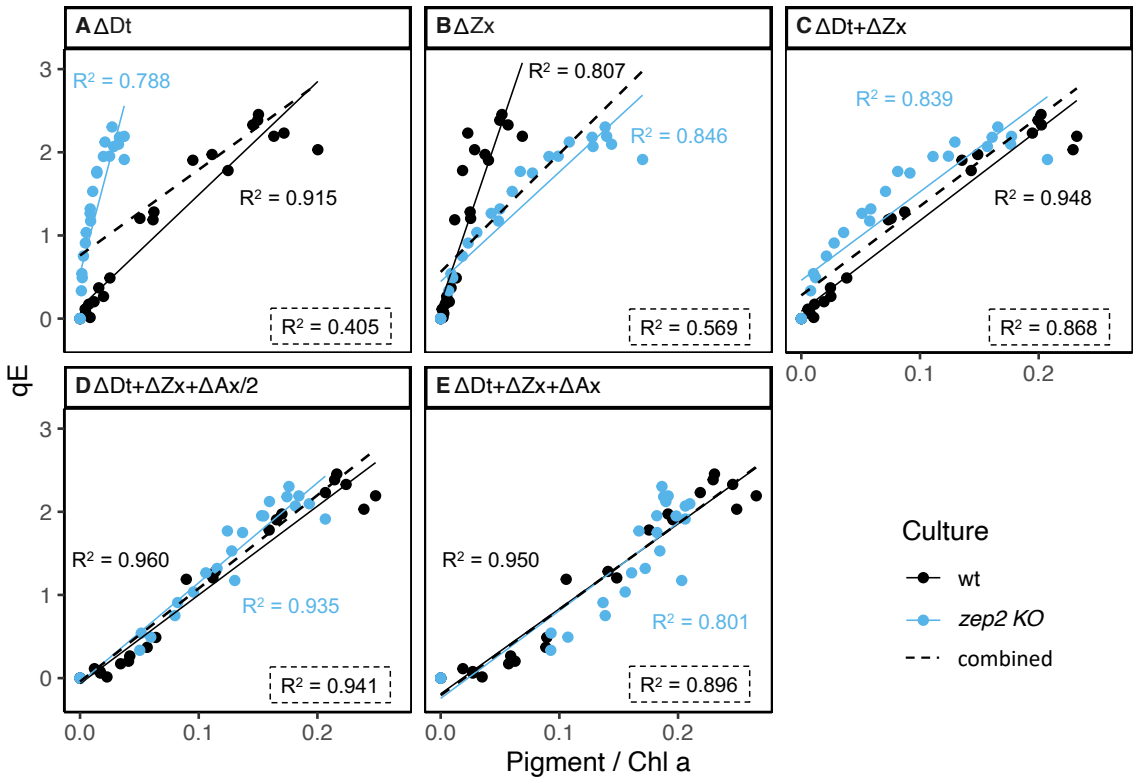

Fig. 6. Correlation between qE and de-epoxidized pigments in wt and *zep2 KO* during recovery from 6 h of HL, on the 5th day of HL:LL exposure. Each point represents a separate measurement, repeated for 3 independent biological replicates. For each strain, different calculations of de-epoxidized pigment pool are displayed, with corresponding linear models and R^2. Dashed lines represent the linear model obtained when considering *zep2 KO* and wt as one unique population (combined); corresponding R^2 is displayed in the dashed text box at the bottom right corner of each facet. (*A*) diadinoxanthin only; (*B*) zeaxanthin only; (*C*) diatoxanthin and

305 zeaxanthin; (*D*) diatoxanthin, zeaxanthin and ½ antheraxanthin; (*E*) diatoxanthin, zeaxanthin and
306 antheraxanthin.

307 **Discussion**

308 In this study, we discovered that pigments of the Vx cycle can contribute to NPQ
309 induction and regulation in algae that normally rely on the Dd cycle, and report that
310 both Zx and Ax can induce NPQ, with the latter having only around half of the
311 quenching-induction capacity of Zx and Dt. Ax participates in the regulation of NPQ
312 in various other photosynthetic eukaryotes, including plants (Gilmore and
313 Yamamoto, 1993; Gilmore et al., 1994; Demmig-Adams and Adams, 1996; Zaks
314 et al., 2013) and green lineage algae (e.g. *Chlorella vulgaris* (Goss et al., 2006b),
315 *Mantoniella squamata* (Goss et al., 1998)). In the heterokont *Nannochloropsis*
316 *oceanica*, Ax contributes to the onset of qE with about 30% efficiency compared
317 to Zx (Short et al., 2023). Moreover, in the giant kelp *Macrocystis pyrifera*, Ax
318 triggers NPQ with half of the efficiency observed for Zx (Ocampo-Alvarez et al.,
319 2013). Brown algae only possess the Vx cycle (García-Mendoza and Colombo-
320 Pallotta, 2007) but display diatom-like qE (i.e., relying directly on the xanthophyll
321 cycle while not being activated by ΔpH alone (Lavaud and Goss, 2014)), likely
322 explaining the similarities with our findings for *P. tricornutum*.
323 Xanthophylls are known to compete for different binding sites within the antennae
324 (Croce et al., 1999; Hobe et al., 2000; Caffarri et al., 2001; Mascoli et al., 2021),
325 and mutants lacking one pigment can substitute it with a closely related one (e.g.,
326 in *A. thaliana* (Kalituho et al., 2007; Dall'Osto et al., 2007) and *C. reinhardtii* (Azadi-
327 Chegeni et al., 2022)). Vx and Dd cycle pigments are highly similar molecules, that
328 differ only due to a triple bond within the isoprenoid backbone of Dd and Dt, that
329 renders their central polyene moiety asymmetrical (**Fig. 1**). As it is established that
330 Dd and Dt must be bound to light harvesting proteins to regulate NPQ (Schumann
331 et al., 2007; Giovagnetti et al., 2022), we propose that Vx, Ax and Zx, when
332 accumulated in favorable concentrations, could occupy the same binding sites thus
333 contributing to qE induction, as indicated by our data (**Fig. 4-6**). Structural
334 differences between the pigments (including the intrinsic asymmetry of Dd and Dt

335 opposed to the symmetric Vx cycle counterparts) could play a role in the
336 differences in quenching efficiency reported between Ax and Dt/Zx.
337 These results suggest that Dt might be equally able to trigger NPQ as Zx/Ax do in
338 taxa that normally rely on the Vx cycle. Once the yet unknown Dd synthase
339 (Dautermann et al., 2020) is discovered, this hypothesis could be tested by
340 implementing the Dd biosynthesis pathway in the green lineage.
341 Xanthophyll cycling is thought to represent an innovation of eukaryotic oxygenic
342 phototrophs, and to have evolved in parallel with light harvesting and other
343 photoprotection strategies (Coesel et al., 2008; Garcia-Mendoza et al., 2011). The
344 Dd cycle most probably evolved in an alga that already possessed the Vx cycle,
345 as Vx is an obligate precursor of Dd and fucoxanthin (Lohr and Wilhelm, 1999;
346 Dautermann et al., 2020; Bai et al., 2022) and VDE and ZEP have sufficiently broad
347 substrate specificities for accepting the xanthophylls from both cycles as
348 substrates (Yamamoto and Higashi, 1978; Bojko et al., 2013; Olchawa-Pajor et al.,
349 2019). According to this scenario, both xanthophyll cycles were functional in the
350 same organism during the early evolution of photosynthetic heterokonts.
351 Extant algae with the Dd cycle still have the potential to accumulate pigments of
352 the Vx cycle (Lohr and Wilhelm, 1999) which, however, is effectively suppressed
353 under most conditions. One explanation for the prevalence of the Dd cycle in these
354 algae could be that Dt is more effective than Zx in triggering NPQ. Our observation
355 that the Vx cycle pigments can efficiently provide NPQ in a modern diatom species
356 that normally relies on the Dd cycle rejects this hypothesis, while it supports the
357 idea of a gradual shift in photoprotection from the Vx to the Dd cycle in heterokont
358 algae.
359 Replacing the two-step Vx cycle with the one-step Dd cycle could provide the
360 benefit of switching faster between NPQ and photosynthetic light harvesting (Lohr
361 and Wilhelm, 1999; Lavaud et al., 2002; Goss et al., 2006a). In support of this
362 hypothesis, our data show that the kinetics of recovery of qE and of xanthophyll
363 re-epoxidation during the first 15 min of recovery are slower in a culture that
364 accumulates primarily Vx cycle pigments (**Fig. 5**). Moreover, the formation of
365 fucoxanthin involves only 5 enzymatic steps from Dt versus 8 steps from Zx (Bai

366 et al., 2022; Cao et al., 2023), thereby also putatively accelerating the conversion
367 of photoprotective xanthophylls accumulated under higher irradiance into light
368 harvesting pigments when light becomes limited. We postulate that a selective
369 advantage conferred by these factors could have contributed to the success of
370 diatoms in dynamic ecosystem such as turbulent waters that are characterized by
371 frequent and extreme light changes (Lavaud, 2007).

372 **Materials and Methods**

373 **CRISPR/Cas9-based gene knockout.** *Phaeodactylum tricornutum* (Pt1;
374 CCAP1055) maintained for several years in our laboratory was used as reference
375 wt and for the generation of all mutant strains. Independent knockout lines (two for
376 *ZEP2* [Phatr2_56488; chr_1:2222646-2224755(+)], and one for *VDE*
377 [Phatr2_44635; chr_4:1116193-1117626(-)] and *ZEP3* [Phatr2_56492;
378 chr_4:1118248-1120587(+)]) were obtained with CRISPR/Cas9 genome editing,
379 through bacterial conjugation. sgRNAs were designed with CRISPOR (Concordet
380 and Haeussler, 2018) and episomal vectors based on pPtPuc3m diaCas9_sgRNA
381 including the respective sgRNA templates were created following previously
382 published methods (Nymark et al., 2017; Sharma et al., 2018). sgRNA coding
383 sequences can be found in **Supplemental Table S3**. Final episomes (containing
384 CRISPR/Cas9 machinery and zeocin resistance cassette) were first transformed
385 into *E. coli* DH10β cells carrying the mobilization helper plasmid pTA-Mob and
386 further introduced into wtPt1 *via* bacterial conjugation, as previously described
387 (Karas et al., 2015; Diner et al., 2016; Sharma et al., 2018).
388 Transformed clones appeared 2-3 weeks after conjugation on agar selection plates
389 (16 g/L salinity f/2 + 100 µg/mL zeocin) incubated at 20°C and 100 µmol photons
390 m^{-2} s^{-1} of white light and were transferred on fresh selection plates (16 g/L salinity
391 f/2 agar + 75 µg/mL zeocin). Screening of mutants followed the strategy previously
392 described (Nymark et al., 2017) and included pre-screening of potentially mutated
393 DNA sequences by PCR amplification via DreamTaq (ThermoFisher Scientific Inc.,
394 Germany) and high-resolution melting curve analysis (HRM) using Biozym HRM
395 PCR Mix (Biozym Scientific GmbH, Germany); primers are listed in **Supplemental**

396 **Table S1**. NPQ phenotypes of the putative mutants were also screened through a
397 chlorophyll *a* fluorescence induction-relaxation protocol (5-10 min light stress at
398 500-600 µmol photons m^{-2} s^{-1} with blue light, followed by recovery at 28 µmol
399 photons m^{-2} s^{-1}) performed with an IMAGING-PAM fluorometer (Heinz Walz
400 GmbH, Germany, described below). For this purpose, cultures were inoculated in
401 well plates with liquid media (16 g/L salinity f/2 + 50 µg/mL zeocin) and grown for
402 3-4 days at 100 µmol photons m^{-2} s^{-1} of white light.
403 After identification of positive candidates, the isolation and screening procedure
404 was repeated 1-3 times to obtain pure monoclonal cultures. We confirmed the
405 mutation in both alleles and the monoclonality of the colonies using TOPO-TA
406 cloning (ThermoFisher Scientific Inc., Germany) followed by sequencing of the
407 individual alleles. Mutated clones with a KO indel on both alleles were selected for
408 experiments. Additional information is available in **Supplemental Note S1**.
409 KO mutants were maintained for several months at 16 °C and 25 µmol photons m^{-}
410 ^{2} s^{-1} of white light with 16:8 h light:dark photoperiod on 16 g/L salinity f/2 agar plates
411 without antibiotic selection, to facilitate the expulsion of the CRISPR/Cas9
412 episome. In addition, prolonged cultivation of transgenic lines was necessary to
413 achieve a stable phenotype before performing experiments, as it is known that in
414 *P. tricornutum* the effects of mutations can be alleviated via compensatory
415 mechanisms such as upregulation of other genes (Nymark et al., 2021). All KO
416 strains generated for this study were later cryopreserved according to (Sprecher
417 et al., 2023).

418 **Complementation of mutant lines.** For each targeted gene (*VDE*, *ZEP2*, and
419 *ZEP3*) we created a modified pPTbsr vector containing the whole length wt gene
420 (amplified from gDNA) with predicted endogenous promoter and terminator to
421 achieve wt-like gene expression. To avoid targeting of the newly inserted
422 sequence, synonymous mutations were introduced at the site of the protospacer
423 adjacent motif in *ZEP2* and *ZEP3*, while a selected episome-free *vde* mutant strain
424 was used for complementation with *VDE*. Biolistic transformation was performed
425 according to (Kroth, 2007). Transformants were grown on selection plates (8 g/L

426 salinity f/2 agar + 4 µg/mL blasticidin-S) for 1-3 weeks at 20°C with 100 µmol
427 photons m^{-2} s^{-1} of white light. DNA of selected clones was extracted as described
428 in (Nymark et al., 2017) and PCR was performed with ALLin™ Mega HiFi DNA
429 Polymerase (highQu GmbH, Germany). PCR products were sequenced
430 (Microsynth, Balgach, Switzerland) and clones showing the insertion of the
431 complete target gene were selected. Primers are listed in **Supplemental Table**
432 **S4**. Complementation lines were then cryopreserved according to (Sprecher et al.,
433 2023).

434 **PCR genotyping.** In absence of a commercial antibody for our target proteins,
435 PCR genotyping with high discrimination polymerase (HiDi, MyPols, Germany)
436 was performed to confirm the purity of all selected lines prior experiments. gDNA
437 was extracted with the same protocol described for transformants screening
438 (Nymark et al., 2017) and amplification was performed according to manufacturer's
439 instructions (with addition of 1 mM $MgCl_2$), using allele-discriminating primers
440 flanking the targeting loci and binding specifically in each line (KO, wt and
441 complemented). Two different primer pairs were used to confirm the presence of
442 both mutated alleles (allele 1 and allele 2) in the KO lines. Primers are listed in
443 **Supplemental Table S1**. PCR products were run on 1% or 2% TAE-agarose gels
444 with 1000 bp or 50 bp GeneRuler (ThermoFisher Scientific Inc., Germany)
445 depending on product size. All gels were stained with ROTI GelStain (Roth Gmbh,
446 Germany). Additional information is available in **Supplemental Note S1**.

447 **Culture conditions.** All experimental strains were maintained in a temperature-
448 controlled growth chamber at 18°C in shaking batch cultures (120-150 rpm).
449 Standard f/2 medium (Guillard, 1975) was prepared with 16 g/L Tropic Marine
450 CLASSIC sea salt (Dr. Biener GmbH, Germany) adjusted to 7.5 pH prior
451 autoclaving. Continuous low light (LL, 30-50 $\mu mol_{photons}$ m^{-2} s^{-1}), measured in
452 culture flask filled with f/2 medium with a ULM-500 light meter with spherical sensor
453 (Heinz Walz GmbH, Germany), was supplied with L 18W/954 LUMILUX®
454 DELUXE Daylight tubes (OSRAM GmbH, Germany).
455 About one week prior to each experiment, cultures were acclimated to semi-

456 chemostatic conditions at 18 °C and continuous LL. For the whole experiment,
457 cultures were maintained at 1-2*10^6 cells/mL in semi-chemostat by daily dilution
458 with fresh medium based on cell counts (Multisizer 4e coulter counter, BECKMAN
459 COULTER, USA).

460 **Experimental setup.** Semi-chemostat cultures acclimated to LL were treated for
461 5 consecutive days with 6 h of high light (HL, 1000-1200 µmol photons m^{-2} s^{-1}
462 measured in f/2 medium, corresponding to ~700 µmol photons m^{-2} s^{-1} in air as
463 used by (Lohr and Wilhelm, 1999), supplied by HO 80W/865 LUMILUX® Cool
464 Daylight, OSRAM GmbH, Germany in addition to the LL lamps), followed by 18 h
465 of LL. For pigments analysis, samples were harvested before (LL control) and after
466 5 days of HL:LL treatment. At the fifth day, cultures were sampled before the onset
467 of the 6 h HL phase (0 h), after 6 h of HL and during recovery in LL (5 and 30 min).
468 Samples (5 mL) were vacuum filtered (ISOPORE™ 1.2 µm PC membrane filters,
469 25 mm), flash-frozen in liquid nitrogen and stored at -80 °C for later analysis with
470 HPLC.
471 To investigate the correlation between the kinetics of xanthophyll cycling and NPQ,
472 the experiment was repeated on *zep* mutants and wt and pigment analysis was
473 coupled with fluorescence measurements. At the fifth day of HL:LL treatment,
474 chlorophyll fluorescence was measured, using an IMAGING-PAM fluorometer
475 (IMAG-S module equipped with IMAG-L LED-Ring-Array and IMAG-K CCD-
476 camera, connected to an IMAG-C control unit, Heinz Walz GmbH, Germany),
477 immediately before the 6 h HL phase (0 h), after 6 h of HL and in the following LL
478 phase after 1, 3, 5, 7.5, 10, 15 and 30 min. The fluorometer was positioned under
479 the light setup (i.e., lamps supplying HL or LL as described above, arranged
480 around the sampling area) without covers, so that the whole sampling and
481 measuring procedure could be performed under the same illumination. Samples
482 (3 mL) were collected from the shaking Erlenmeyer flasks and immediately
483 transferred into a 24-well plate that was positioned below the CCD-camera of the
484 fluorometer, while still receiving the same experimental light (i.e., HL or LL as
485 defined above) during the measurements. Blue actinic illumination from the

486 IMAGING-PAM was never supplied to the cultures, while a weak blue pulse-
487 modulated measuring light (low repetition rate, ca. 1 Hz) was applied to measure
488 chlorophyll fluorescence without altering the photophysiological state of the
489 samples. A saturating pulse of blue light from the IMAGING-PAM (max intensity:
490 3000 µmol photons m^{-2} s^{-1}; width: 800 ms) was supplied to measure maximum
491 fluorescence at each time point described above. Simultaneously, samples (5 mL)
492 were collected from the same Erlenmeyer flasks for pigment analysis and
493 preserved as described above. This approach allowed to determine a precise
494 pigment-NPQ correlation under our experimental conditions. NPQ (Fm-Fm′/Fm′)
495 was derived defining Fm as the maximum fluorescence obtained at the first LL
496 pulse (0 h) (Murchie and Lawson, 2013). Instead of darkness, we considered LL
497 as condition in which the maximum of reaction centers are opened, since in
498 diatoms NPQ is not relaxed in the dark (Lepetit et al., 2013). To isolate its effect
499 from the photoinhibition-related quenching (qI), qE (i.e., the rapidly relaxing
500 component of NPQ, also indicated as qZ in diatoms) was calculated as Fm''-
501 Fm'/Fm', where Fm'' corresponds to the maximum fluorescence at the end of the
502 recovery phase (30 min) (Blommaert et al., 2021). Similarly, corresponding deltas
503 for xanthophyll cycle pigments were calculated as Δp = [p]-[p]'', where [p]
504 corresponds to the pigment concentration at a given time point, and [p]'' at the end
505 of the recovery phase (30 min).

506 **Pigment analysis (HPLC).** Pigments extraction was performed as in (Buck et al.,
507 2019). Samples (80 µL) were separated on a NUCLEOSIL® C18 column (EC
508 250/4, 300-5, MACHEREY-NAGEL GmbH, Germany) in a LaChrome Elite HPLC
509 equipped with an L-2130 pump module, L-2455 diode array detector, and L-2200
510 autosampler (VWR International, Germany). Elution was performed at 0.8 mL/min
511 flow rate using a three-phase gradient consisting of eluent A (85% methanol, 15%
512 0.5M ammonium acetate in water), B (90% acetonitrile, 10% water), and C (100%
513 ethyl acetate) following the protocol established by (Kraay et al., 1992). Classical
514 diatom pigments were identified from known absorption spectra and retention
515 times (Roy et al., 2011) and quantified using the integrated absorption peak area

516 at 440 nm and previously determined conversion factors. Retention times and λ_{max}
517 for each pigment and representative chromatograms for each mutant are reported
518 in **Supplemental Table S2, Fig. S5**. For Vx cycle pigments, preliminary
519 identification was further confirmed via spiking with pure crystalline standards (DHI
520 group, Hørsholm, Denmark). If detected, content of chlorophyllide *a* was always
521 summed to that of chlorophyll *a*. Preliminary data assessment was performed with
522 EZChrome *Elite* (Agilent, USA) and OpenChrome (Lablicate Gmbh, Germany)
523 (Wenig and Odermatt, 2010).

524 **Transient expression of *P. tricornutum ZEP2* and *ZEP3* in a ZEP-deficient**
525 **tobacco mutant.** Full-length *ZEP2* and *ZEP3* from *P. tricornutum* strain UTEX 646
526 were PCR-amplified from cDNA using Phusion High-Fidelity DNA Polymerase
527 (Thermo Scientific, Carlsbad, USA) and subcloned into the pGEM-T® Easy Vector
528 (Promega, Mannheim, Germany). PCR-related mutations were excluded by
529 confirming that sequences of the cloned genes were identical to sequencing
530 results from PCR products. For generation of plasmids for *Agrobacterium*-
531 mediated tobacco transformation, the gene fragments encoding the mature
532 proteins were PCR amplified, subcloned into pGEM®-T Easy, excised with AvrII
533 and PacI and ligated into the AvrII and PacI sites of plasmid pPZPbar-tp_{AtZEP}-
534 AtZEP (Dautermann and Lohr, 2017), thereby replacing the ZEP gene from
535 *Arabidopsis thaliana* and yielding plasmids pPZPbar-tp_{AtZEP}-PtZEP2 and pPZPbar-
536 tp_{AtZEP}-PtZEP3. Growth of the ZEP-deficient *aba2* mutant of tobacco *N.*
537 *plumbaginifolia* (Marin et al., 1996), the *Agrobacterium*-mediated transformation of
538 tobacco leaves with the pPZPbar constructs of *AtZEP*, *PtZEP2* and *PtZEP3*,
539 sampling and pigment analysis of lyophilized tobacco leaf discs was performed as
540 described before (Dautermann and Lohr, 2017). All analyses were done at least in
541 triplicate from independent transformants, with the HPLC chromatograms showing
542 representative results.

543 **Data analysis and statistics.** DNA and protein sequences were analyzed with
544 Geneious 9.1 (Biomatters, New Zealand, 2016). Analysis of pigment and
545 chlorophyll *a* fluorescence data was performed with R 4.2.1 (R foundation for

statistical computing, Vienna, Austria). Multiple comparison t-tests were performed to test differences in average pigment content and NPQ between mutant lines and wt at different time points; adjusted p-values (Holm correction for multiple comparisons) were used to evaluate statistical significance. Normality was evaluated prior with a combination of graphical methods (Q-Q plot, residual analysis) and Shapiro-Wilk test. For qE/Δpigment correlations, linear regressions were modeled with a standard linear model function. Model fit was evaluated with graphical methods (Q-Q plot, residual analysis) and R^2. Finally, xanthophyll cycle and qE recovery kinetics were fitted in Microsoft Excel and Origin respectively, using first order kinetics equations (Laidler, 1970). For xanthophyll cycle rates, at each time point molar ratios of pigment/chlorophyll *a* were normalized to the total pool size of each xanthophyll cycle individually. To exclude the influence of *de novo* biosynthesis processes taking place during the 6 h of HL, we excluded data points corresponding to the beginning of the HL phase (0 h) from qE/Δpigment correlations and from kinetic rates calculations.

Funding

B.L. received funding from DFG (German Research Fundation, Bonn, Germany; LE 3358/3-2 and Heisenberg program). C.E.G. acknowledges Studienstiftung des Deutschen Volkes (Bonn, Germany) for funding her doctoral scholarship.

Author Contributions

C.E.G. and B.L. designed the project; C.E.G., M.L. and B.L. designed experiments; A.F.S., M.A.W., and J.M.B. generated constructs for CRISPR-Cas KO and complementation lines; C.E.G., B.L. and M.A.W. generated and screened the mutant lines; C.E.G. performed experiments on *P. tricornutum* and analyzed the data; M.L. calculated and analyzed the xanthophyll cycle's kinetics. O.D. generated constructs for and performed the experiments on *Nicotiana plumbaginifolia*; C.E.G., M.A.W., P.G.K., M.L., and B.L. concluded the final data interpretation; C.E.G. wrote the initial draft of the manuscript, edited by B.L. and

M.L.; The manuscript was revised and completed with contribution of all authors.

Declaration of interest

The authors declare no competing interest.

Acknowledgments

The authors acknowledge Benjamin Bailleul for his support in NPQ modelling. We also thank Annette Ramsperger for her contribution to the generation of mutant lines, and Alexander H. Fürst, Selina Pucher and Manuel Müller for their help during preliminary characterization and genotyping of the mutants, in the aim of a practical course. Finally, C.E.G thanks Prof. David Schleheck for the project discussions.

Data and strains availability statement

Mutant algal strains are cryopreserved in the laboratory of Prof. Peter Kroth (Department of Biology, University of Konstanz, 78457 Konstanz, Germany) and are available upon request. Additional queries can be addressed to the corresponding authors.

References

Azadi-Chegeni, F., Thallmair, S., Ward, M. E., Perin, G., Marrink, S. J., Baldus, M., Morosinotto, T., and Pandit, A. (2022). Protein dynamics and lipid affinity of monomeric, zeaxanthin-binding LHCII in thylakoid membranes. *Biophys J* **121**:396–409.

Bai, Y., Cao, T., Dautermann, O., Buschbeck, P., Cantrell, M. B., Chen, Y., Lein, C. D., Shi, X., Ware, M. A., Yang, F., et al. (2022). Green diatom mutants reveal an intricate biosynthetic pathway of fucoxanthin. *Proceedings of the National Academy of Sciences* **119**.

598 **Bailleul, B., Rogato, A., De Martino, A., Coesel, S., Cardol, P., Bowler, C.,**
599 **Falciatore, A., and Finazzi, G.** (2010). An atypical member of the light-
600 harvesting complex stress-related protein family modulates diatom
601 responses to light. *Proc Natl Acad Sci U S A* **107**:18214–18219.

602 **Baroli, I., Do, A. D., Yamane, T., and Niyogi, K. K.** (2003). Zeaxanthin
603 accumulation in the absence of a functional xanthophyll cycle protects
604 *Chlamydomonas reinhardtii* from photooxidative stress. *Plant Cell* **15**:992–
605 1008.

606 **Bassi, R., and Dall'Osto, L.** (2021). Dissipation of Light Energy Absorbed in
607 Excess: The Molecular Mechanisms. *Annu Rev Plant Biol* **72**:47–76.

608 **Biswal, B.** (1995). Carotenoid catabolism during leaf senescence and its control
609 by light. *J Photochem Photobiol B* **30**:3–13.

610 **Blommaert, L., Chafai, L., and Bailleul, B.** (2021). The fine-tuning of NPQ in
611 diatoms relies on the regulation of both xanthophyll cycle enzymes. *Sci Rep*
612 **11**:1–16.

613 **Bojko, M., Olchawa-Pajor, M., Tuleja, U., Kuczyńska, P., Strzałka, W.,**
614 **Latowski, D., and Strzałka, K.** (2013). Expression of three diadinoxanthin
615 de-epoxidase genes of *Phaeodacylum tricornutum* in *Escherichia coli*
616 Origami b and BL21 strain. *Acta Biochim Pol* **60**:857–60.

617 **Buck, J. M., Sherman, J., Bártulos, C. R., Serif, M., Halder, M., Henkel, J.,**
618 **Falciatore, A., Lavaud, J., Gorbunov, M. Y., Kroth, P. G., et al.** (2019).
619 Lhcx proteins provide photoprotection via thermal dissipation of absorbed
620 light in the diatom *Phaeodactylum tricornutum*. *Nat Commun* **10**.

621 **Buck, J. M., Kroth, P. G., and Lepetit, B.** (2021). Identification of sequence
622 motifs in Lhcx proteins that confer qE-based photoprotection in the diatom
623 *Phaeodactylum tricornutum*. *The Plant Journal* **108**:1721–1734.

624 **Caffarri, S., Croce, R., Breton, J., and Bassi, R.** (2001). The major antenna
625 complex of Photosystem II has a xanthophyll binding site not involved in light
626 harvesting. *Journal of Biological Chemistry* **276**:35924–35933.

627 **Cao, T., Bai, Y., Buschbeck, P., Tan, Q., Cantrell, M. B., Chen, Y., Jiang, Y.,**
628 **Liu, R.-Z., Ries, N. K., Shi, X., et al.** (2023). An unexpected hydratase
629 synthesizes the green light-absorbing pigment fucoxanthin. *Plant Cell*
630 **35**:3053–3072.

631 **Coesel, S., Oborník, M., Varela, J., Falciatore, A., and Bowler, C.** (2008).
632 Evolutionary origins and functions of the carotenoid biosynthetic pathway in
633 marine diatoms. *PLoS One* **3**.

634 **Concordet, J. P., and Haeussler, M.** (2018). CRISPOR: Intuitive guide selection
635 for CRISPR/Cas9 genome editing experiments and screens. *Nucleic Acids*
636 *Res* **46**:W242–W245.

637 **Croce, R., Weiss, S., and Bassi, R.** (1999). Carotenoid-binding sites of the
638 major light-harvesting complex II of higher plants. *Journal of Biological*
639 *Chemistry* **274**:29613–29623.

640 **Croteau, D., Guérin, S., Bruyant, F., Ferland, J., Campbell, D. A., Babin, M.,**
641 **and Lavaud, J.** (2021). Contrasting nonphotochemical quenching patterns
642 under high light and darkness aligns with light niche occupancy in Arctic
643 diatoms. *Limnol Oceanogr* **66**:S231–S245.

644 **Dall'Osto, L., Cazzaniga, S., North, H., Marion-Poll, A., and Bassi, R.** (2007).
645 The *Arabidopsis* aba4-1 mutant reveals a specific function for neoxanthin in
646 protection against photooxidative stress. *Plant Cell* **19**:1048–1064.

647 **Dambek, M., Eilers, U., Breitenbach, J., Steiger, S., Büchel, C., and**
648 **Sandmann, G.** (2012). Biosynthesis of fucoxanthin and diadinoxanthin and
649 function of initial pathway genes in *Phaeodactylum tricornutum*. *J Exp Bot*
650 **63**:5607–5612.

651 **Dautermann, O., and Lohr, M.** (2017). A functional zeaxanthin epoxidase from
652 red algae shedding light on the evolution of light-harvesting carotenoids and
653 the xanthophyll cycle in photosynthetic eukaryotes. *Plant Journal* **92**:879–
654 891.

655 **Dautermann, O., Lyska, D., Andersen-Ranberg, J., Becker, M., Fröhlich-**
656 **Nowoisky, J., Gartmann, H., Krämer, L. C., Mayr, K., Pieper, D., Rij, L.**
657 **M., et al.** (2020). An algal enzyme required for biosynthesis of the most
658 abundant marine carotenoids. *Sci Adv* **6**.

659 **Demmig-Adams, B., and Adams, W. W.** (1996). The role of xanthophyll cycle
660 carotenoids in the protection of photosynthesis. *Trends Plant Sci* **1**:21–26.

661 **Diner, R. E., Bielinski, V. A., Dupont, C. L., Allen, A. E., and Weyman, P. D.**
662 (2016). Refinement of the diatom episome maintenance sequence and
663 improvement of conjugation-based DNA delivery methods. *Front Bioeng*
664 *Biotechnol* **4**.

665 **Domingues, N., Matos, A. R., da Silva, J. M., and Cartaxana, P.** (2012).
666 Response of the Diatom *Phaeodactylum tricornutum* to photooxidative stress
667 resulting from high light exposure. *PLoS One* **7**.

668 **Eilers, U., Dietzel, L., Breitenbach, J., Büchel, C., and Sandmann, G.** (2016).
669 Identification of genes coding for functional zeaxanthin epoxidases in the
670 diatom *Phaeodactylum tricornutum*. *J Plant Physiol* **192**:64–70.

671 **Falkowski, P. G., Katz, M. E., Knoll, A. H., Quigg, A., Raven, J. A., Schofield,**
672 **O., and Taylor, F. J. R.** (2004). The Evolution of Modern Eukaryotic
673 Phytoplankton. *Science (1979)* **305**:354–360.

674 **Field, C. B., Behrenfeld, M. J., Randerson, J. T., and Falkowski, P. G.** (1998).
675 Primary Production of the Biosphere: Integrating Terrestrial and Oceanic
676 Components. *Science (1979)* **281**:237–240.

677 **Frommolt, R., Werner, S., Paulsen, H., Goss, R., Wilhelm, C., Zauner, S.,**
678 **Maier, U. G., Grossman, A. R., Bhattacharya, D., and Lohr, M.** (2008).
679 Ancient recruitment by chromists of green algal genes encoding enzymes for
680 carotenoid biosynthesis. *Mol Biol Evol* **25**:2653–2667.

681 **García-Mendoza, E., and Colombo-Pallotta, M. F.** (2007). The giant kelp
682 *Macrocystis pyrifera* presents a different nonphotochemical quenching
683 control than higher plants. *New Phytologist* **173**:526–536.

684 **Garcia-Mendoza, E., Ocampo-Alvarez, H., and Govindjee** (2011).
685 Photoprotection in the brown alga *Macrocystis pyrifera*: Evolutionary
686 implications. *J Photochem Photobiol B* **104**:377–385.

687 **Gilmore, A. M., and Yamamoto, H. Y.** (1993). Linear models relating
688 xanthophylls and lumen acidity to non-photochemical fluorescence
689 quenching. Evidence that antheraxanthin explains zeaxanthin-independent
690 quenching. *Photosynth Res* **35**:67–78.

691 **Gilmore, A. M., Mohanty, N., and Yamamoto, H. Y.** (1994). Epoxidation of
692 zeaxanthin and antheraxanthin reverses non-photochemical quenching of
693 photosystem II chlorophyll a fluorescence in the presence of trans-thylakoid
694 ΔpH. *FEBS Lett* **350**:271–274.

695 **Giovagnetti, V., Jaubert, M., Shukla, M. K., Ungerer, P., Bouly, J. P.,**
696 **Falciatore, A., and Ruban, A. V.** (2022). Biochemical and molecular
697 properties of LHCX1, the essential regulator of dynamic photoprotection in
698 diatoms. *Plant Physiol* **188**:509–525.

699 **Goss, R., and Lepetit, B.** (2015). Biodiversity of NPQ. *J Plant Physiol* **172**:13–
700 32.

701 **Goss, R., Böhme, K., and Wilhelm, C.** (1998). The xanthophyll cycle of
702 *Mantoniella squamata* converts violaxanthin into antheraxanthin but not to
703 zeaxanthin: consequences for the mechanism of enhanced non-
704 photochemical energy dissipation. *Planta* **205**:613–621.

705 **Goss, R., Ann Pinto, E., Wilhelm, C., and Richter, M.** (2006a). The importance
706 of a highly active and ΔpH-regulated diatoxanthin epoxidase for the
707 regulation of the PS II antenna function in diadinoxanthin cycle containing
708 algae. *J Plant Physiol* **163**:1008–1021.

709 **Goss, R., Lepetit, B., and Wilhelm, C.** (2006b). Evidence for a rebinding of
710 antheraxanthin to the light-harvesting complex during the epoxidation
711 reaction of the violaxanthin cycle. *J Plant Physiol* **163**:585–590.

712 **Græsholt, C., Brembu, T., Volpe, C., Bartosova, Z., Serif, M., Winge, P., and**
713 **Nymark, M.** (2024). Zeaxanthin epoxidase 3 Knockout Mutants of the Model
714 Diatom *Phaeodactylum tricornutum* Enable Commercial Production of the
715 Bioactive Carotenoid Diatoxanthin. *Mar Drugs* **22**.

716 **Grouneva, I., Jakob, T., Wilhelm, C., and Goss, R.** (2009). The regulation of
717 xanthophyll cycle activity and of non-photochemical fluorescence quenching
718 by two alternative electron flows in the diatoms *Phaeodactylum tricornutum*
719 and *Cyclotella meneghiniana*. *Biochim Biophys Acta Bioenerg* **1787**:929–
720 938.

721 **Guillard, R. R. L.** (1975). Culture of Phytoplankton for Feeding Marine
722 Invertebrates. In *Culture of Marine Invertebrate Animals*, pp. 29–60. Boston,
723 MA: Springer US.

724 **Hobe, S., Niemeier, H., Bender, A., and Paulsen, H.** (2000). Carotenoid
725 binding sites in LHCIIb. *Eur J Biochem* **267**:616–624.

726 **Kalituho, L., Rech, J., and Jahns, P.** (2007). The roles of specific xanthophylls
727 in light utilization. *Planta* **225**:423–439.

728 **Kan, C., Zhao, Y., Sun, K., Tang, X., and Zhao, Y.** (2023). The inhibition and
729 recovery mechanisms of the diatom *Phaeodactylum tricornutum* in response
730 to high light stress – A study combining physiological and transcriptional
731 analysis. *J Phycol* **59**:418–431.

Karas, B. J., Diner, R. E., Lefebvre, S. C., McQuaid, J., Phillips, A. P. R., Noddings, C. M., Brunson, J. K., Valas, R. E., Deerinck, T. J., Jablanovic, J., et al. (2015). Designer diatom episomes delivered by bacterial conjugation. *Nat Commun* **6**.

Kraay, G. W., Zapata, M., and Veldhuis, M. J. W. (1992). Separation of chlorophylls *c1*, *c2*, and *c3* of marine phytoplankton by reversed-phase C18 high-performance liquid chromatography. *J Phycol* **28**:708–712.

Kroth, P. G. (2007). Genetic Transformation. In *Protein Targeting Protocols* (ed. van der Giezen, M.), pp. 257–267. Totowa, NJ: Humana Press.

Kuczynska, P., Jemiola-Rzeminska, M., Nowicka, B., Jakubowska, A., Strzalka, W., Burda, K., and Strzalka, K. (2020). The xanthophyll cycle in diatom *Phaeodactylum tricornutum* in response to light stress. *Plant Physiology and Biochemistry* **152**:125–137.

Laidler, K. J. (1970). *Reaction Kinetics*. Elsevier Science & Technology.

Latowski, D., Kuczyńska, P., and Strzałka, K. (2011). Xanthophyll cycle – a mechanism protecting plants against oxidative stress. *Redox Report* **16**:78–90.

Lavaud, J. (2007). Fast Regulation of Photosynthesis in Diatoms: Mechanisms, Evolution and Ecophysiology. *Functional Plant Science and Biotechonology* **1**:267–287.

Lavaud, J., and Goss, R. (2014). The Peculiar Features of Non-Photochemical Fluorescence Quenching in Diatoms and Brown Algae. In *Non-Photochemical Quenching and Energy Dissipation in Plants, Algae and Cyanobacteria* (ed. Demmig-Adams, B.), Garab, G.), Adams III, W.), and Govindjee), pp. 421–443. Springer Dordrecht.

Lavaud, J., Rousseau, B., and Etienne, A.-L. (2002). In diatoms, a transthylakoid proton gradient alone is not sufficient to induce a non-photochemical fluorescence quenching. *FEBS Lett* **523**:163–166.

Lavaud, J., Strzepek, R. F., and Kroth, P. G. (2007). Photoprotection capacity differs among diatoms: Possible consequences on the spatial distribution of diatoms related to fluctuations in the underwater light climate. *Limnol Oceanogr* **52**:1188–1194.

Lavaud, J., Materna, A. C., Sturm, S., Vugrinec, S., and Kroth, P. G. (2012). Silencing of the violaxanthin de-epoxidase gene in the diatom *Phaeodactylum tricornutum* reduces diatoxanthin synthesis and non-photochemical quenching. *PLoS One* **7**.

Lepetit, B., Sturm, S., Rogato, A., Gruber, A., Sachse, M., Falciatore, A., Kroth, P. G., and Lavaud, J. (2013). High light acclimation in the secondary plastids containing diatom *Phaeodactylum tricornutum* is triggered by the redox state of the plastoquinone pool. *Plant Physiol* **161**:853–865.

Lepetit, B., Gélin, G., Lepetit, M., Sturm, S., Vugrinec, S., Rogato, A., Kroth, P. G., Falciatore, A., and Lavaud, J. (2017). The diatom *Phaeodactylum tricornutum* adjusts nonphotochemical fluorescence quenching capacity in response to dynamic light via fine-tuned Lhcx and xanthophyll cycle pigment synthesis. *New Phytologist* **214**:205–218.

Lohr, M. (2011). Carotenoid metabolism in phytoplankton. In *Phytoplankton Pigments* (ed. Roy, S.), Llewellyn, C.), Egeland, E. S.), and Johnsen, G.), pp. 113–162. Cambridge: Cambridge University Press.

Lohr, M., and Wilhelm, C. (1999). Algae displaying the diadinoxanthin cycle also possess the violaxanthin cycle. *Proc Natl Acad Sci U S A* **96**:8784–8789.

Lohr, M., and Wilhelm, C. (2001). Xanthophyll synthesis in diatoms: quantification of putative intermediates and comparison of pigment

784 conversion kinetics with rate constants derived from a model. *Planta*
785 **212**:382–391.

786 **Marin, E., Nussaume, L., Quesada, A., Gonneau, M., Sotta, B., Hugueney, P.,**
787 **Frey, A., and Marion-Poll, A.** (1996). Molecular identification of zeaxanthin
788 epoxidase of Nicotiana plumbaginifolia, a gene involved in abscisic acid
789 biosynthesis and corresponding to the ABA locus of Arabidopsis thaliana.
790 *EMBO J* **15**:2331–2342.

791 **Mascoli, V., Liguori, N., Cupellini, L., Elias, E., Mennucci, B., and Croce, R.**
792 (2021). Uncovering the interactions driving carotenoid binding in light-
793 harvesting complexes. *Chem Sci* **12**:5113–5122.

794 **Murchie, E. H., and Lawson, T.** (2013). Chlorophyll fluorescence analysis: A
795 guide to good practice and understanding some new applications. *J Exp Bot*
796 **64**:3983–3998.

797 **Nymark, M., Valle, K. C., Brembu, T., Hancke, K., Winge, P., Andresen, K.,**
798 **Johnsen, G., and Bones, A. M.** (2009). An integrated analysis of molecular
799 acclimation to high light in the marine diatom *Phaeodactylum tricornutum*.
800 *PLoS One* **4**.

801 **Nymark, M., Sharma, A., Hafskjold, M., Sparstad, T., Bones, A., and Winge,**
802 **P.** (2017). CRISPR/Cas9 Gene Editing in the Marine Diatom *Phaeodactylum*
803 *tricornutum*. *Bio Protoc* **7**:1–12.

804 **Nymark, M., Grønbech Hafskjold, M. C., Volpe, C., Fonseca, D. de M.,**
805 **Sharma, A., Tsirvouli, E., Serif, M., Winge, P., Finazzi, G., and Bones, A.**
806 **M.** (2021). Functional studies of CpSRP54 in diatoms show that the
807 mechanism of thylakoid protein insertion differs from that in plants and green
808 algae. *Plant Journal* **106**:113–132.

809 **Ocampo-Alvarez, H., García-Mendoza, E., and Govindjee** (2013). Antagonist
810 effect between violaxanthin and de-epoxidated pigments in

811 nonphotochemical quenching induction in the qE deficient brown alga
812 *Macrocystis pyrifera*. *Biochim Biophys Acta Bioenerg* **1827**:427–437.

813 **Olchawa-Pajor, M., Bojko, M., Strzalka, W., Strzalka, K., and Latowski, D.**
814 (2019). Violaxanthin conversion by recombinant diatom and plant de-
815 epoxidases, expressed in *Escherichia coli* – a comparative analysis. *Acta*
816 *Biochim Pol* **66**:249–255.

817 **Roy, S., Llewellyn, C., Egeland, E. S., and Johnsen, G.** (2011). *Phytoplanton*
818 *Pigments - Characterization, Chemotaxonomy and Applications in*
819 *Oceanography Pigments*. Cambridge University Press.

820 **Schumann, A., Goss, R., Jakob, T., and Wilhelm, C.** (2007). Investigation of
821 the quenching efficiency of diatoxanthin in cells of *Phaeodactylum*
822 *tricornutum* (Bacillariophyceae) with different pool sizes of xanthophyll cycle
823 pigments. *Phycologia* **46**:113–117.

824 **Sharma, A. K., Nymark, M., Sparstad, T., Bones, A. M., and Winge, P.** (2018).
825 Transgene-free genome editing in marine algae by bacterial conjugation –
826 comparison with biolistic CRISPR/Cas9 transformation. *Sci Rep* **8**:1–11.

827 **Short, A., Fay, T. P., Crisanto, T., Mangal, R., Niyogi, K. K., Limmer, D. T.,**
828 **and Fleming, G. R.** (2023). Kinetics of the xanthophyll cycle and its role in
829 photoprotective memory and response. *Nat Commun* **14**.

830 **Sprecher, B. N., Buck, J. M., Ropella, L. L., Ramsperger, A., Kroth, P. G.,**
831 **and Yamada, N.** (2023). Genetic transformation methods for diatom
832 *Nitzschia captiva*: New tools to better understand dinotom endosymbiosis.
833 *Algal Res* **72**:103136.

834 **Steiger, S., Schäfer, L., and Sandmann, G.** (1999). High-light-dependent
835 upregulation of carotenoids and their antioxidative properties in the
836 cyanobacterium *Synechocystis* PCC 6803. *J Photochem Photobiol B* **52**:14–
837 18.

838 **Takahashi, S., and Badger, M. R.** (2011). Photoprotection in plants: a new light
839 on photosystem II damage. *Trends Plant Sci* **16**:53–60.

840 **Tozzi, S., Schofield, O., and Falkowski, P. G.** (2004). Historical climate change
841 and ocean turbulence as selective agents for two key phytoplankton
842 functional groups. *Mar Ecol Prog Ser* **274**:123–132.

843 **Ware, M. A., Paton, A. J., Bai, Y., Kassaw, T., Lohr, M., and Peers, G.** (2024).
844 Identifying the gene responsible for NPQ reversal in *Phaeodactylum*
845 *tricornutum*. *bioRxiv* Advance Access published January 1, 2024,
846 doi:10.1101/2024.03.27.587055.

847 **Wenig, P., and Odermatt, J.** (2010). OpenChrom: A cross-platform open source
848 software for the mass spectrometric analysis of chromatographic data. *BMC*
849 *Bioinformatics* **11**.

850 **Wilhelm, C., Büchel, C., Fisahn, J., Goss, R., Jakob, T., LaRoche, J.,**
851 **Lavaud, J., Lohr, M., Riebesell, U., Stehfest, K., et al.** (2006). The
852 Regulation of Carbon and Nutrient Assimilation in Diatoms is Significantly
853 Different from Green Algae. *Protist* **157**:91–124.

854 **Yamamoto, H. Y., and Higashi, R. M.** (1978). Violaxanthin de-epoxidase: Lipid
855 composition and substrate specificity. *Arch Biochem Biophys* **190**:514–522.

856 **Zaks, J., Amarnath, K., Sylak-Glassman, E. J., and Fleming, G. R.** (2013).
857 Models and measurements of energy-dependent quenching. *Photosynth*
858 *Res* **116**:389–409.

859